The effect of KF post-deposition treatments on the optoelectronic properties of $Cu(In,Ga)Se_2$ single crystals

Omar Ramírez, Maud Bertrand, Alice Debot, Daniel Siopa, Nathalie Valle, Jörg Schmauch, Michele Melchiorre and Susanne Siebentritt*

O. Ramírez, M. Bertrand, A. Debot, D. Siopa, Dr. M. Melchiorre, Prof. S. Siebentritt
Department of Physics and Materials Science, University of Luxembourg, 41 rue du Brill, L-4422, Belvaux, Luxembourg
E-mail: omar.ramirez@uni.lu

Dr. N. Valle
Luxembourg Institute of Science and Technology—Materials Research and Technology Department, 41 rue du Brill, L-4422, Belvaux, Luxembourg

J. Schmauch
Experimental Physics, Saarland University, 66123 Saarbrücken, Germany.

Keywords: CIGSe, single crystals, grain boundaries, alkali post-deposition treatments, photoluminescence.

The power conversion efficiency boost of $Cu(In,Ga)Se_2$ in the past years has been possible due to the incorporation of heavy alkali atoms. Their addition through post-deposition treatments results in an improvement of the open-circuit voltage, which origin has been associated with grain boundaries. The present work discusses the effect of potassium fluoride post-deposition treatments on the optoelectronic properties of a series of sodium-free $Cu(In,Ga)Se_2$ single crystals with varying Cu and Ga content. Results suggest that improvement of the quasi-Fermi level splitting can be achieved despite the absence of grain boundaries, being greater in low-gallium Cu-poor absorbers. Secondary ion mass spectrometry reveals the presence of potassium inside the bulk of the films, suggesting that transport of potassium can occur through grain interiors. In addition, a type inversion from n to p in KF-treated low-gallium $Cu(In,Ga)Se_2$ is observed, which along a carrier lifetime study demonstrates that potassium can act as a dopant. The fact that potassium by its own can alter the optoelectronic properties of $Cu(In,Ga)Se_2$ single crystals demonstrates that the effect of post-deposition treatments goes beyond grain boundary passivation.

1. Introduction

Thin film solar cells based on the chalcopyrite $Cu(In,Ga)Se_2$ have seen a constant boost in their power conversion efficiency due, among other reasons, to the incorporation of heavy alkali metals in the form of post-deposition treatments.[1-3] Effective alkali incorporation into $Cu(In,Ga)Se_2$ absorbers results in an improvement of the short-circuit current density (J_{SC}) and the open-circuit voltage (V_{OC}); the first one has been associated with modifications of the absorbers' surface that allows a reduction in the CdS buffer layer thickness, bringing down its parasitic absorption.[1] The V_{OC} improvement, on the other hand, has been associated with modifications in the bulk, where the role of the grain boundaries has been demonstrated to be of great importance.[4-7] The preferential segregation of alkali elements at grain boundaries has been confirmed by several groups and measured by means of atom probe tomography.[8-10] This fact has led to the association of alkali elements with a passivating effect at grain boundaries, which has found experimental backup by reports of reduced band bending[5] and lower tail state density.[7] On the other hand, it has been shown that neither sodium nor potassium have an impact on the recombination velocities at grain boundaries, suggesting that the alkalis do not have a passivating effect.[11] The effect of grain boundaries in polycrystalline $Cu(In,Ga)Se_2$ has led to a number of studies to investigate their physics and role in device performance[12-14].

We aim to understand the role of grain boundaries by comparing the known effects on polycrystalline films with the effect of alkali post-deposition treatments in single crystalline films, which do not have grain boundaries. Studies on single crystals of the ternaries $CuInSe_2$ and $CuGaSe_2$ outnumber the ones found in literature for the quaternary $Cu(In,Ga)Se_2$, and most of them have focused on the electronic structure, crystal quality and the interaction between the chalcopyrite and the substrate used for the growth.[15-17] It was not until 2018 that Nishinaga et. al. demonstrated the capability of $Cu(In,Ga)Se_2$ single crystals grown by molecular beam epitaxy to accomplish power conversion efficiencies of 20%. Such improvement was achieved by implementing some of the techniques used in polycrystalline absorbers like a Ga gradient

and the combination of a NaF and KF post-deposition treatments. In that study, the role of Na was attributed to a doping effect (as already reported by Pianezzi et.al.[18]) while in the case of K, to an improved $Cu(In,Ga)Se_2$-CdS interface. Moreover, the authors found no evidence of K diffusion into the bulk, fact that was attributed to the absence of grain boundaries.

A plausible explanation on the discrepancies found in literature when assessing the effectiveness of PDTs, is the fact that it can be influenced by the composition of the $Cu(In,Ga)Se_2$ absorber. The Cu content[19] as well as the ratio of group III elements[20-21] seem to play an important role for the outcome of the alkali PDT; which would imply that samples with differences in stoichiometry, Ga gradients, presence of ordered vacancy compounds, among others, would yield different results even if they were subjected to the same post-deposition treatment.

In this contribution, we study the effect of potassium fluoride post-deposition treatments on the optoelectronic properties of $Cu(In,Ga)Se_2$ single crystals grown by metalorganic vapor phase epitaxy. The use of sodium-free single crystals allowed us to investigate the sole effect that potassium would have in the grain interiors when there is neither sodium nor grain boundaries present. In addition, the influence of the copper as well as the gallium content on the effectiveness of the PDTs is assessed by means of quasi Fermi level splitting (qFls). A difference of more than 30meV in qFls was obtained after the KF-PDT, suggesting that potassium can be incorporated into $Cu(In,Ga)Se_2$ despite the absence of grain boundaries. Also, we demonstrate that potassium acts as a dopant causing a type inversion from n to p in the case of Cu-poor low-gallium absorbers, as previously observed with sodium in pure $CuInSe_2$ by Werner et. al.[22] Furthermore, we observe dependency on the copper and gallium content of the effectiveness of the KF post-deposition treatment, being more effective in Cu-poor and having no effect in Cu-rich low-gallium absorbers. The effectiveness of PDTs depending on the composition has also been reported for polycrystalline absorbers[19-20]. Thus, our study shows that the observed effect is not grain boundary-related. A photoluminescence study including

time-resolved and low-temperature measurements is presented. Several other characterization techniques such as secondary ion mass spectrometry (SIMS), electron backscatter diffraction (EBSD), X-ray diffraction (XRD), conductivity and Seebeck coefficient measurements are also performed to support our findings. The fact that heavier alkali metals like potassium have the ability to alter the optoelectronic properties of sodium-free $Cu(In,Ga)Se_2$ single crystals suggests that heavy alkali post-deposition treatments have a positive effect not only at the grain boundaries but also on the grain interiors.

2. Results and Discussion

Several single crystalline thin films grown by MOVPE and with varying composition were used to investigate the effects of potassium fluoride post-deposition treatments on the optoelectronic properties of $Cu(In,Ga)Se_2$. The study is divided into three sections: in the first part, we demonstrate that our films are single crystals and that no unintended grain boundaries are present; later, the effectiveness of the KF-PDT depending on the copper content for a Ga content of 40% is investigated and finally, samples with low gallium content are studied.

2.1. $Cu(In,Ga)Se_2$ Single Crystals

When growing heteroepitaxial films, one of the most important aspects to take in consideration is the lattice mismatch between the single crystal used as a substrate and the intended material to be grown. GaAs, with a lattice constant *a* of 5.653Å at room temperature[23] is a suitable substrate for the growth of the chalcopyrite $Cu(In_{1-x},Ga_x)Se_2$ which has a lattice constant *a* ranging from 5.777Å for x = 0 to 5.604Å for x = 1.[24] It is also possible for the *c*-axis of the tetragonal chalcopyrite structure to grow parallel to the GaAs surface in order to reduce the lattice mismatch, which is expected for $0.22 < x < 0.54$ when $c/2$ is closer to the GaAs lattice constant than the lattice parameter *a*. Minimizing the lattice mismatch is of great importance as failing to do so would result in the accumulation of tensile or compressive strain that would

need to be released in the form of line, planar or bulk defects.[25] High gallium CIGSe single crystals grown on Zn doped p+-type GaAs(001) by molecular beam epitaxy, for example, were found to contain orthogonal cross-hatch features oriented along the <100> direction of the CIGSe film and other kind of defects as a result of the tensile strain built up during film growth.[26] The problem with growing GaAs-matched $Cu(In_{1-x},Ga_x)Se_2$ is that in order to do so, it would be necessary to use rather high Ga contents ($x \approx 0.68$ for *a*-matched and $x \approx 0.48$ for *c*/2-matched), which is not characteristic of state of the art devices. In the present study, most of the samples involved were grown with an average gallium content of $x \approx 0.4$ as a compromise between lattice mismatch and the Ga content usually employed in high-efficiency devices ($x \approx 0.3$).

A cross-section image of one of the samples used in this study is depicted in **Figure 1**(a), where it is possible to appreciate that no random grain boundaries are present in the film. More cross-section images and top-views of other samples studied can be found in the supplementary information Figure S1. Another way to corroborate that we are not dealing with polycrystalline absorbers is by means of X-ray diffraction. Figure 1(b) displays the diffractogram of two selected samples with different gallium content used in this study; both samples show the characteristic peak at 66.1° corresponding to the (400) of GaAs (PDF 00-014-0450), as well as the (008) of $Cu(In_{1-x},Ga_x)Se_2$ at around 64.6° for the sample with $x < 0.1$ and 65.5° for $x \sim 0.4$.[27] The difference observed in 2θ for the peak position of the (008) reflection when comparing with the references (63.9 and 65.8° for $x = 0$ and $x = 0.5$, respectively) comes from the Ga content. Polycrystalline absorbers display a strong reflection from the 112 plane as it has the highest structure factor (see the powder diffraction files below for reference). We find that none of the samples show a reflection from 26.5 to 27.1° as can be seen in the logarithmic inset of Figure 1(b), which is the expected 2θ range for the 112 plane from pure $CuInSe_2$ to $Cu(In_{0.5},Ga_{0.5})Se_2$ according to the PDF 01-070-3356 and 00-062-0055, respectively (more XRD data can be found in the supplementary information Figure S2). Additionally, an electron

backscatter diffraction analysis of two samples with different Cu content was carried out revealing no grain boundaries over several thousand square micrometers (Figure S3 of the supplementary information).

For the purpose of this contribution, it was also necessary to study samples without a Ga gradient, as changes in the notch position along the film could influence the results. A SIMS analysis was performed to corroborate the Ga profile, which was confirmed to be rather flat as depicted in Figure 1(c). The intensities obtained from the measurement were normalized and multiplied by each element's atomic percentage determined from EDX. Non-intentional diffusion of Ga from the GaAs wafer towards the front seems to occur due to the elevated temperatures of the growth process (520°C), as already described by Schroeder et.al.[15], but is essentially limited to within 50 nm. However, all the samples are expected to be equally affected as the growth conditions of temperature and pressure were kept the same, allowing its direct comparison since the Ga gradient is negligible.

Thus, the combination of these measurements confirms that our films are in fact single crystals with a nearly constant Ga/(Ga+In) across the film thickness.

2.2. Cu Influence

For the study of the copper influence on the effectiveness of the KF-PDT, it was important to make sure that no significant difference in the group III elements was present among the samples so the sole effect of the copper content could be assessed. Energy-dispersive X-ray spectroscopy was employed to determine the elemental composition and the results are listed in Table S1 of the supplementary material. **Figure 2**(a) summarizes the extracted Cu/(In+Ga) (CGI) and Ga/(Ga+In) (GGI) ratios. The eight single crystals used in the Cu-series have an average Ga content of 42±2%, a thickness of 700 to 800nm and a Cu/(In+Ga) ratio ranging from 0.73 to 1.04. It is important to notice that samples 1 and 2 have a Cu/(In+Ga) below 0.8, which according to the phase diagram no longer corresponds to a pure chalcopyrite phase but a

mixed chalcopyrite and ordered vacancy compounds (OVCs).[28] The presence of such OVCs was confirmed by Raman spectroscopy (Figure S4 of the supplementary information) where, besides the main peak at 178 cm^{-1} corresponding to the A1 mode of $Cu(In,Ga)Se_2$, a peak with lower intensity at 153 cm^{-1} associated with the $CuIn_3Se_5$ OVC is observed.[29-30]

In order to assess the effect of the KF-PDT, photoluminescence spectroscopy was used to determine the quasi-Fermi level splitting (qFls) of each sample before and after receiving the KF-PDT. The normalized spectra of all samples taken at room temperature can be seen in Figure 2(b): a difference of 60 meV in the PL peak position between the most Cu-poor and the stoichiometric sample can be observed. Since the Ga/(Ga+In) of these two samples is quite similar, this difference in bandgap is mostly related to the Cu content.[31] The broadening of the peak towards lower Cu contents is also characteristic of Cu-poor $Cu(In,Ga)Se_2$ and caused by potential fluctuations originated from the high degree of compensation [32-33].

The qFls can be considered as the internal voltage of the absorber. The external voltage (the open circuit voltage V_{OC}) of the completed cell, contains also the influence of interfaces and contacts and can be lower than the qFls.[34] However, it has been demonstrated that the V_{OC} is almost equal to the qFls in state of the art $Cu(In,Ga)Se_2$ devices.[35] The qFls of each sample was determined from a linear fit to the high-energy wing of the PL spectrum as explained in [35-38]. For each sample, four measurements were recorded at different positions and the extracted qFls averaged (qFls values can be found in the supplementary information Table S2). The difference in qFls (ΔqFls) between samples that received the KF-PDT and the as-grown state is shown in **Figure 3**(a). At first glance, a strong relationship between the Cu content and the effect of the KF-PDT on qFls can be noticed: a decrease in qFls for Cu/(Ga+In) below 0.8, and an increasing effect towards higher Cu contents. A similar trend in V_{OC} was observed by Kodalle et.al. when studying rubidium fluoride PDTs on polycrystalline $Cu(In,Ga)Se_2$, where they correlated the availability of Cu vacancies with the formation of a Rb-In-Se secondary phase, which was found detrimental for device performance[19].

A change in qFls can be linked to the electron or the hole quasi-Fermi level shifting. In a p-type semiconductor, a change in the electron quasi-Fermi level (E_{Fn}) would relate to a change in the minority carrier concentration, i.e. reduced recombination centers, while a change in the hole quasi-Fermi level (E_{Fp}) to the majority carrier, i.e. the doping level, considering a low injection case[39].

In order to figure out the origin of the observed changes in qFls, a time-resolved photoluminescence (TRPL) study was conducted on four selected samples. The TRPL decays were fitted by a 2-exponential model, both the KF-treated samples' decays and their fit are depicted in Figure 3(b). τ_2 was taken as the effective lifetime as it has been reported to better describe recombination in the bulk.[40] Longer lifetimes were obtained for the lowest Cu contents. The extracted lifetimes before and after KF-PDT are compared in Figure 3(c). Hardly any changes in lifetime were measured, ruling out the possibility of a decrease in non-radiative recombination centers to be the reason for the observed improvement in qFls after the KF-PDT. Since E_{Fn} is not shifting upwards, it is reasonable to assume that the observed improvement in qFls is related to E_{Fp} moving downwards. In order to corroborate our assumption, the conductivity of the same four samples investigated with TRPL was measured. As can be seen in Figure 3(d), all four samples show an increase in conductivity after the KF-PDT. The conductivity of a semiconductor σ depends on the carrier concentration N and the mobility μ, and (for a p-type semiconductor) is given by $\sigma = q\mu_p N_A$, where q is the elementary charge and N_A the acceptor concentration.

Even though we cannot rule out a possible change in the mobility, an increase in carrier concentration of one order of magnitude (like in the case of the sample with a Cu/(Ga+In) of 0.95) would be more expected than the same amount of change in mobility. A similar trend in conductivity was observed by Contreras et.al. when studying the influence of alkali metals in polycrystalline $Cu(In,Ga)Se_2$. Furthermore, they report that no significant changes in mobility were detected by Hall measurements in their experiments [41].

So far, an increase in carrier concentration could explain the improvement by the KF treatment observed in the samples with Cu/(Ga+In) higher than 0.8 but cannot explain the behavior of samples with lower Cu contents. In this case, an increase in both conductivity and minority carrier lifetime after the KF treatment should yield an improvement in qFls as well, which is contrary to what we observe. One aspect to keep in mind is that the KF-PDT is done in a Se atmosphere, which might have a separate effect on the optoelectronic properties of the films. We discuss potential reasons for this behavior below.

It should be noted that during MOVPE growth the Se pressure is rather low, compared to the growth by co-evaporation.[42] In order to have a better understanding of the sole effect of the KF-PDT and compare with the effects on polycrystalline films, all samples are compared with Se-treated absorbers instead of the as-grown state. It has been reported that Se-PDTs can impact the solar cell performance of polycrystalline co-evaporated $Cu(In,Ga)Se_2$ in a beneficial or detrimental way, depending on the absence or presence of sodium, respectively. [43] Furthermore, Se-PDTs have been demonstrated to have a beneficial impact on passivating surface defects in Cu-rich $CuInSe_2$.[44] Since we cannot provide selenium during the cool-down stage of the MOVPE process, it is reasonable to assume that a Se-PDT could also have an effect on the absorbers. **Figure 4** displays the change in qFls between the KF-treated and the Se-treated samples. This experiment demonstrates that the Se-PDT has indeed an effect on the absorbers, and that the previously observed trend on the effect of the KF-PDT with respect to the as-grown state is altered when comparing the KF-treated samples to Se-treated ones. For Cu contents above 0.83, a beneficial effect of the Se-PDT is observed when compared to as-grown samples (Figure S5 of the supporting information), in agreement with the report by Barreau et.al. for Na-free polycrystalline CIGSe with Cu/(Ga+In)~0.9. [43] For Cu contents below 0.8, however, a considerable qFls loss is measured. Since these samples contain OVCs, we can just speculate that its presence plays a role dictating the outcome of the treatment. For example, it could be possible that OVCs promote the confinement of carriers due to their larger

bandgap, which is partially lifted after the Se-PDT. It has been reported that alkali post-deposition treatments, for example, lead to a reduction of such defect compounds[45].

In fact, this new comparison (KF-PDT vs Se-PDT) demonstrates that the KF-PDT has a stronger effect in very Cu-poor samples since an average gain in qFls of 15meV is obtained for Cu/(Ga+In) up to 0.8 and just 7meV for Cu contents between 0.8 and 1.0. The trend observed for Cu-poor samples when comparing KF and Se-treated absorbers in Figure 4, resembles the one of the density of intrinsic copper vacancies (V_{Cu}) in $CuInSe_2$ measured by neutron powder diffraction.[46] Stephan et.al. found a quite constant density of V_{Cu} in the Cu/In region between 0.8 and 1 and a higher density of almost one order of magnitude when OVCs were present. Based on these results, we can speculate that the higher density of V_{Cu} present in Cu contents below 0.8 facilitated the diffusion of potassium, resulting in the larger improvement observed in lower Cu contents. The fact that the formation energy of the substitutional defect K_{Cu} is the lowest among other possible configurations[47] also supports this model. The relevance of OVCs in effective KF-PDTs has been similarly described by Lepetit et.al. in polycrystalline CIGSe, where it was found that the presence of such compounds on the surface was indeed crucial to achieve a favorable effect of the PDT.[48] Interestingly, the improvement of 17meV observed in the sample with Cu/(Ga+In) = 1.03 suggests that the effect of the KF-PDT in the Cu-rich regime has another origin, as for this Cu content the density of V_{Cu} is considerably lower.

In summary, the effectiveness of KF-PDTs has been found to be strongly dependent on the Cu/(Ga+In) ratio. Our results suggest that comparing KF-treated samples with as-grown references can be misleading, and that a Se-treated reference instead is more suitable to assess the real effect of the PDT. KF-PDTs were found to be more effective in Cu contents below 0.8, a fact attributed to a higher density of copper vacancies and ordered vacancy compounds. The observed improvement in qFls for all copper contents was demonstrated to be bulk-related and associated with an increase in carrier concentration.

2.3. Cu influence in low-Ga absorbers

In the previous section, we demonstrated that the KF-PDT can have an effect on the qFls depending on the Cu content and that such change is most likely related to an increase in the net doping. The small yet meaningful change in qFls obtained when comparing KF-treated with Se-treated samples, made us question the impact of the high Ga content used in the Cu-series and its possible relation with the observed changes. It is worth mentioning that the electronic quality of the single-crystals used in the study is comparable (regardless of the Ga/(Ga+In) ratio), since the quasi-Fermi level splitting loss with respect to the Shockley-Queisser V_{OC} did not change considerably with the gallium content (Figure S6 of the supporting information).

A study by Ishizuka et.al. demonstrated that the group III elemental composition of the absorber strongly dictates the outcome of RbF-PDTs.[20] They found that the improvement in V_{OC} after the PDT was stronger in $CuInSe_2$ than in $Cu(In,Ga)Se_2$, and almost negligible in pure $CuGaSe_2$. This result is in agreement with our finding of a rather small improvement due to KF in films with 40% Ga/(Ga+In). This observation could be related to the unfavorable band alignment of CdS with high-gallium $Cu(InGa)Se_2$, which could induce interface recombination as the dominant recombination path. A favorable band alignment is however possible with Zn(O,S).[49] In order to make sure that the limitations of the improvement observed after the KF-PDT in these high Ga absorbers is indeed bulk-related and not due to the interface with the CdS buffer layer, two of the studied samples were covered with Zn(O,S) instead. Regardless of the buffer layer utilized, the improvement in qFls after the KF-PDT was basically the same (ΔqFls values can be found in the supporting information Table S3). This observation indicates that the limited effect of KF on high Ga absorbers is indeed a bulk effect.

Such finding motivated us to study $Cu(In,Ga)Se_2$ single crystals with a low gallium content. Three samples with Cu-poor, stoichiometric and Cu-rich composition and a Ga/(Ga+In) ratio below 0.1 are studied. A table listing the atomic percentages obtained from EDX can be found in the supplementary material (the samples are referenced in Table S1 as samples 9, 10 and 11).

The stoichiometric sample presented a radial compositional gradient that was characterized with EDX. Twelve points were measured from the center (point 1) towards the edge (point 12) of the wafer, and the determined Cu/(Ga+In) is plotted in **Figure 5**(a) along with a schematic representation of the sample. The center was found to have a higher Cu content than the edge. Two pieces of this wafer containing both the edge and center were treated with KF-PDT and Se-only PDT, respectively. Since the PL yield is largely affected by compositional variations, a line scan of the PL main transition (around 1 eV) at room temperature was taken along 20mm of sample starting at the center of the wafer (less Cu-poor). The radius of the laser used for the measurement is around 1.3mm and each measurement was taken every 500µm, assuring the complete coverage of the sample by the line scan. Figure 5(b) and (c) show the PL line scan spectra of the Se-PDT and KF-PDT samples, respectively. A clear increase of the PL yield towards the edge of the wafer (that corresponds to the lower Cu content) is obvious, whereas no significant change can be observed closer to the stoichiometric point. The average difference in qFls ($qFls_{KF}$-$qFls_{Se}$) for the first 5mm of sample is around 4meV, while in the last 5mm (corresponding to the most Cu-poor side) ΔqFls is ~20meV.

The previous experiment indicates that in low gallium Cu(In,Ga)Se_2, the KF-PDT has a more substantial effect and also a stronger relation between Cu content and its effectiveness compared to the ~42% gallium experiment from the previous section. In order to verify this observation, a Cu-poor and a Cu-rich sample with Cu/(Ga+In) of 0.86 and 1.12, respectively, were studied. First, a PL spectrum at 10K was recorded for each sample and is displayed in **Figure 6**(a). Cu-poor and Cu-rich low gallium CIGSe possess very distinct signatures at 10K. In the case of the sample grown under Cu excess, several peaks can be observed, which are assigned to an excitonic emission (Exc) right below the bandgap and two donor-acceptor pairs (DA) with their respective phonon replica, confirming that the film is Cu-rich.[17] The indium-rich sample on the other hand, shows the characteristic redshifted asymmetric broad peak of Cu-poor material[50-52].

Once the composition of both samples was confirmed, they were KF-treated and their qFls determined. It is worth mentioning that the elemental composition by EDX was determined after the growth, while the PL analysis was performed after the samples were KCN etched, ruling out any possible effect of secondary phases in the measured spectra. In the case of the Cu-rich crystal, no change in the PL yield was obtained after the KF-PDT when comparing to a Se-treated reference. A figure displaying several PL spectra taken at room temperature before and after the KF-PDT can be found in the supplementary information Figure S7. In the case of the Cu-poor sample on the contrary, a gain of 30meV in qFls after the KF-PDT was obtained as can be seen from the PL yield difference in Figure 6(b). When investigating the origin of this improvement, the lifetime of both samples was calculated by TRPL (supplementary information Figure S8). Opposite to what we had previously observed for the 40% Ga-containing samples of the previous section, the lifetime of the Cu-poor KF-treated sample increased by a factor of two. This change in lifetime cannot explain the improvement of 30meV in qFls as a factor of two would only account for ~17meV due to the non-radiative loss. Additionally, comparing minority carrier lifetimes only makes sense if the conductivity type does not change. $CuInSe_2$ grown in the absence of sodium can result in either an n-type or a p-type semiconductor depending on the Cu/In ratio: n-type for Cu-poor and p-type for Cu-rich.[22, 53-56] Since the Cu-poor sample contains only a small fraction of Ga, it was expected to be an n-type semiconductor; fact that was confirmed by determining the Seebeck coefficient. After the KF-PDT, the conductivity was found to change to p-type, as shown in Figure 6(c). As already observed for the Ga containing samples: the KF-PDT increases the p-type doping.

A type inversion from n to p can happen by either increasing the acceptor or reducing the donor concentration. In the $CuInSe_2$ system, the acceptor concentration is dictated mainly by the shallow V_{Cu} and Cu_{In} while In_{Cu} and Cu-interstitials account for the donors (for a comprehensive insight on electronic defects in $Cu(In,Ga)Se_2$, see the review by Spindler et.al.[52]). We attribute the observed type inversion to an increased acceptor concentration due

to a potassium-related defect as SIMS revealed the presence of potassium along the absorber layer (Figure 6(d)). Theoretical results suggest that potassium substituting indium sites (K_{In}) would actually act as an acceptor with a formation energy even lower than the K_{Cu} in the case of an n-type semiconductor, which is the case presented herein.[47] The fact that a type inversion occurred as a result of the KF-PDT implies that potassium can effectively alter the electronic structure of $Cu(In,Ga)Se_2$ and, since all the presented experiments were performed on single crystals, that even without grain boundaries a bulk effect of heavy alkali post-deposition treatments can be observed.

3. Conclusion

The effect of potassium fluoride post-deposition treatments was demonstrated in a set of $Cu(In,Ga)Se_2$ single crystals grown by MOVPE. The effectiveness of the treatment depending on the absorber composition was studied and assessed by means of quasi-Fermi level splitting (qFls).

We find that in the absence of sodium, potassium on its own does alter the optoelectronic properties of $Cu(In,Ga)Se_2$. Furthermore, we find that in order to relate the effect of the KF-PDT on these MOVPE-grown samples with the effect of KF-PDT in polycrystalline absorbers, a comparison between KF-treated and Se-only treated absorbers would be more appropriate (instead of comparing with the as-grown state), as the Se-PDT by itself has an influence on the absorber's properties. In terms of composition, a strong relationship between Cu and Ga content and the effectiveness of the KF-PDT was observed. In the case of $Cu(In,Ga)Se_2$ with a Ga content of ~40%, an average improvement of 15meV and 7meV was achieved for Cu/(Ga+In) ratios below 0.8 and between 0.8 and 1, respectively. We associate the larger improvement observed for the most Cu-poor samples to the higher availability of Cu vacancies caused by the presence of ordered vacancy compounds. A TRPL study of the KF-treated samples revealed no changes in the minority carrier's lifetime, suggesting that the improvement observed in qFls

does not originate from a reduction in non-radiative recombination centers, but from changes in the doping level, which is corroborated by the increased conductivity after the treatment.

Low gallium (below 10%) $Cu(In,Ga)Se_2$ was also studied. We find that absorbers grown under Cu excess (Cu/In > 1), show no improvement in qFls after receiving the KF-PDT. However, the effect on Cu-poor samples was double the one observed in high Ga absorbers (~30meV). Furthermore, a type inversion from n to p caused by the KF-PDT was observed, which made us conclude that in the absence of sodium, potassium acts as a dopant.

The ability of potassium to diffuse and alter the electronic structure of $Cu(In,Ga)Se_2$, regardless the absence of random grain boundaries, demonstrates that the effect of heavy alkali post-deposition treatments goes beyond grain boundary passivation.

4. Experimental Section

Heteroepitaxial Growth: $Cu(In_{1-x},Ga_x)Se_2$ single crystals were grown by metalorganic vapor phase epitaxy (MOVPE) on 500μm thick (100)-oriented semi-insulating GaAs wafers. The reactor temperature and pressure were set at 520°C and 90mbar for all the processes. The metalorganic precursors used were cyclopentadienyl-coppertriethyl phosphine (CpCuTEP), trimethylindium (TMIn), triethylgallium (TEGa) and diisopropylselenide (DiPSe). In order to achieve the desired composition, the CpCuTEP partial pressure was kept constant and the partial pressures of TMIn and TEGa adjusted for each process. The partial pressure of the selenide precursor was chosen so all processes had a similar selenium overpressure of Se/M~25. In the case of the absorbers with less than 10% gallium content, a 100nm thick buffer layer of $Cu(In_{0.6},Ga_{0.4})Se_2$ was grown at the beginning of the process to reduce the strain caused by lattice mismatch with GaAs.

KF post-deposition treatments: After growth, each sample was cleaved in a N_2-filled glovebox and transferred into an MBE chamber where potassium fluoride was evaporated at a rate of roughly 1nm/min during 6 minutes. The KF deposition was done under a Se pressure of ~$2x10^{-}$

^{6} Torr at a substrate temperature of 350°C. After the treatment, the samples were rinsed with DI water and etched in a 5% KCN solution right before the CdS buffer layer deposition. In the case of the samples with CGI > 1, a 10% KCN solution was used instead in order to remove any Cu_xSe secondary phases.

Photoluminescence: Measurements were performed using a 660nm diode laser with a spot diameter of ~2.6mm as excitation source. Two parabolic mirrors were used to collect and redirect the emitted photoluminescence into a spectrometer where it was detected by an InGaAs array. All measurements for qFls determination were carried out at room temperature and spectrally corrected using a calibrated halogen lamp. For the spectra taken at 10K, a liquid helium flow cryostat was used. For the determination of the quasi-Fermi level splitting, the value was extracted from a linear fit of the high-energy wing of the emitted PL (described by Planck's generalized law with the Boltzmann approximation).[36] Time resolved photoluminescence (TRPL) measurements were taken with a LifeSpec II Spectrometer equipped with a 640nm pulsed diode laser.

Chemical, structural and electrical characterization: Secondary Ion Mass Spectrometry (SIMS) depth profiles were obtained with a CAMECA SC-Ultra instrument. The spectrometer was operating at 1keV with a focused Cs^+ ion beam (5 nA) over a surface of 250 μm by 250 μm. Ions of interest were detected as MCs^+ or $MCs_2^+$where M stands for O, Na, K, As, Cu, In, Ga, Se and F. They were collected from an area of 60 μm^2 centered on the scanned area. The sputtering time was converted into apparent depth based on cross-section SEM images, which were taken with a Hitachi SU-70 field-emission scanning electron microscope. Elemental composition was determined by energy dispersive X-ray spectroscopy (EDX) taken at 7kV. Raman measurements were taken with a Renishaw inVia micro spectrometer at room temperature with a 532nm laser excitation focused on the sample with a 50× objective lens and a numerical aperture of 0.5, in combination with a 2400 lines/mm grating. A silicon reference was used for calibration.

The electron backscatter diffraction (EBSD) analysis was performed using a JEOL 7000F SEM equipped with an EDAX/TSL analysis system. The Kikuchi pattern was generated at an acceleration voltage of 15 kV and a beam current of 5nA recorded by a Digiview camera system. JCPDS file number 351102 corresponding to a $CuIn_{0.7}Ga_{0.3}Se_2$ was used for the indexing of the EBSD maps. The X-ray diffraction (XRD) measurements were carried out in Bragg-Brentano configuration with Cu Kα radiation in the 2θ range from 20° to 90° on a Bruker D8 Advance Discover V2 with a step of 0.02°. Resistivity measurements were performed according to the Van der Pauw formalism.

Supporting Information
Supporting Information is available from the Wiley Online Library or from the author.

Acknowledgements

This work was supported by the Luxembourgish Fond National de la Recherche in the framework of the projects: GRISC, STARSOL and MASSENA. We acknowledge and thank Dr. Renaud Leturcq from the Luxembourg Institute of Science and Technology for all his support regarding the Seebeck coefficient measurements. We also thank M. Sood for the Zn(O,S) deposition, B. El Adib for SIMS measurements and Dr. T. Weiss for the fruitful TRPL discussions.

Received: ((will be filled in by the editorial staff))
Revised: ((will be filled in by the editorial staff))
Published online: ((will be filled in by the editorial staff))

References

[1] A. Chirilă, P. Reinhard, F. Pianezzi, P. Bloesch, A. R. Uhl, C. Fella, L. Kranz, D. Keller, C. Gretener, H. Hagendorfer, D. Jaeger, R. Erni, S. Nishiwaki, S. Buecheler, A. N. Tiwari, *Nat. Mater.* **2013**, 12, 1107.
[2] P. Jackson, D. Hariskos, R. Wuerz, W. Wischmann, M. Powalla, *Phys. Status Solidi RRL* **2014**, 8, 219.
[3] P. Jackson, R. Wuerz, D. Hariskos, E. Lotter, W. Witte, M. Powalla, *Phys. Status Solidi RRL* **2016**, 10, 583.
[4] N. Nicoara, T. Lepetit, L. Arzel, S. Harel, N. Barreau, S. Sadewasser, *Sci. Rep.* **2017**, 7, 41361.
[5] N. Nicoara, R. Manaligod, P. Jackson, D. Hariskos, W. Witte, G. Sozzi, R. Menozzi, S. Sadewasser, *Nat. Commun.* **2019**, 10, 3980.

[6] C. P. Muzzillo, *Sol. Energy Mater. Sol. Cells* **2017**, 172, 18.
[7] S. Siebentritt, E. Avancini, M. Bär, J. Bombsch, E. Bourgeois, S. Buecheler, R. Carron, C. Castro, S. Duguay, R. Félix, E. Handick, D. Hariskos, V. Havu, P. Jackson, H.-P. Komsa, T. Kunze, M. Malitckaya, R. Menozzi, M. Nesladek, N. Nicoara, M. Puska, M. Raghuwanshi, P. Pareige, S. Sadewasser, G. Sozzi, A. N. Tiwari, S. Ueda, A. Vilalta-Clemente, T. P. Weiss, F. Werner, R. G. Wilks, W. Witte, M. H. Wolter, *Adv. Energy Mater.* **2020**, 10, 1903752.
[8] P. Schöppe, S. Schönherr, R. Wuerz, W. Wisniewski, G. Martínez-Criado, M. Ritzer, K. Ritter, C. Ronning, C. S. Schnohr, *Nano Energy* **2017**, 42, 307.
[9] O. Cojocaru-Mirédin, P. Choi, D. Abou-Ras, S. S. Schmidt, R. Caballero, D. Raabe, *IEEE J. Photovolt.* **2011**, 1, 207.
[10] A. Laemmle, R. Wuerz, T. Schwarz, O. Cojocaru-Mirédin, P.-P. Choi, M. Powalla, *J. Appl. Phys.* **2014**, 115, 154501.
[11] D. Abou-Ras, A. Nikolaeva, S. Caicedo Dávila, M. Krause, H. Guthrey, M. Al-Jassim, M. Morawski, R. Scheer, *Sol. RRL.* **2019**, 3, 1900095.
[12] U. Rau, K. Taretto, S. Siebentritt, *Appl. Phys. A* **2008**, 96, 221.
[13] S. Siebentritt, M. Igalson, C. Persson, S. Lany, *Prog Photovolt.* **2010**, 18, 390.
[14] D. Abou-Ras, C. T. Koch, V. Küstner, P. A. van Aken, U. Jahn, M. A. Contreras, R. Caballero, C. A. Kaufmann, R. Scheer, T. Unold, H. W. Schock, *Thin Solid Films* **2009**, 517, 2545.
[15] D. J. Schroeder, G. D. Berry, A. A. Rockett, *Appl. Phys. Lett.* **1996**, 69, 4068.
[16] D. Colombara, F. Werner, T. Schwarz, I. Cañero Infante, Y. Fleming, N. Valle, C. Spindler, E. Vacchieri, G. Rey, M. Guennou, M. Bouttemy, A. G. Manjón, I. Peral Alonso, M. Melchiorre, B. El Adib, B. Gault, D. Raabe, P. J. Dale, S. Siebentritt, *Nat. Commun.* **2018**, 9, 826.
[17] N. Rega, S. Siebentritt, J. Albert, S. Nishiwaki, A. Zajogin, M. C. Lux-Steiner, R. Kniese, M. J. Romero, *Thin Solid Films* **2005**, 480-481, 286.
[18] F. Pianezzi, P. Reinhard, A. Chirilă, B. Bissig, S. Nishiwaki, S. Buecheler, A. N. Tiwari, *Phys. Chem. Chem. Phys.* **2014**, 16, 8843.
[19] T. Kodalle, T. Bertram, R. Schlatmann, C. A. Kaufmann, *IEEE J. Photovolt.* **2019**, 9, 1839.
[20] S. Ishizuka, N. Taguchi, J. Nishinaga, Y. Kamikawa, S. Tanaka, H. Shibata, *J. Phys. Chem. C* **2018**, 122, 3809.
[21] N. H. Valdes, K. J. Jones, R. L. Opila, W. N. Shafarman, *IEEE J. Photovolt.* **2019**, 9, 1846.
[22] F. Werner, D. Colombara, M. Melchiorre, N. Valle, B. El Adib, C. Spindler, S. Siebentritt, *J. Appl. Phys.* **2016**, 119, 173103.
[23] E. D. Pierron, D. L. Parker, J. B. McNeely, *Acta Cryst.* **1966**, 21, 290.
[24] T. Tinoco, C. Rincón, M. Quintero, G. S. Pérez, *Phys. Status Solidi A* **1991**, 124, 427.
[25] C. H. Lei, A. A. Rockett, I. M. Robertson, N. Papathanasiou, S. Siebentritt, *J. Appl. Phys.* **2006**, 100, 114915.
[26] H. Guthrey, A. Norman, J. Nishinaga, S. Niki, M. Al-Jassim, H. Shibata, *ACS Appl. Mater. Interfaces* **2020**, 12, 3150.
[27] N. Rega, S. Siebentritt, I. Beckers, J. Beckmann, J. Albert, M. Lux-Steiner, *J. Cryst. Growth* **2003**, 248, 169.
[28] T. Gödecke, Haalboom, T., and Ernst, F, *Z. Metallkd* **2000**, 91, 622.
[29] C.-M. Xu, X.-L. Xu, J. Xu, X.-J. Yang, J. Zuo, N. Kong, W.-H. Huang, H.-T. Liu, *Semicond. Sci. Technol.* **2004**, 19, 1201.
[30] C. Rincón, F. J. Ramírez, *J. Appl. Phys.* **1992**, 72, 4321.
[31] L. Gütay, D. Regesch, J. K. Larsen, Y. Aida, V. Depredurand, A. Redinger, S. Caneva, S. Schorr, C. Stephan, J. Vidal, S. Botti, S. Siebentritt, *Phys. Rev. B* **2012**, 86, 045216.

[32] S. Siebentritt, L. Gütay, D. Regesch, Y. Aida, V. Deprédurand, *Sol. Energy Mater. Sol. Cells* **2013**, 119, 18.
[33] I. Dirnstorfer, M. Wagner, D. M. Hofmann, M. D. Lampert, F. Karg, B. K. Meyer, *Phys. Status Solidi A* **1998**, 168, 163.
[34] F. Babbe, L. Choubrac, S. Siebentritt, *Sol. RRL.* **2018**, 2, 1800248.
[35] M. H. Wolter, B. Bissig, E. Avancini, R. Carron, S. Buecheler, P. Jackson, S. Siebentritt, *IEEE J. Photovolt.* **2018**, 8, 1320.
[36] F. Babbe, L. Choubrac, S. Siebentritt, *Appl. Phys. Lett.* **2016**, 109, 082105.
[37] A. Lomuscio, T. Rödel, T. Schwarz, B. Gault, M. Melchiorre, D. Raabe, S. Siebentritt, *Phys. Rev. Appl.* **2019**, 11, 054052.
[38] L. Gütay, G. H. Bauer, *Thin Solid Films* **2009**, 517, 2222.
[39] D. Adeleye, A. Lomuscio, M. Sood, S. Siebentritt, *J. Phys. Condens. Matter* **2020**, Submitted.
[40] T. P. Weiss, B. Bissig, T. Feurer, R. Carron, S. Buecheler, A. N. Tiwari, *Sci. Rep.* **2019**, 9, 5385.
[41] M. A. Contreras, B. Egaas, P. Dippo, J. Webb, J. Granata, K. Ramanathan, S. Asher, A. Swartzlander, R. Noufi, presented at Conference Record of the Twenty Sixth IEEE Photovoltaic Specialists Conference - 1997, 29 Sept.-3 Oct. 1997, **1997**.
[42] F. Babbe, H. Elanzeery, M. H. Wolter, K. Santhosh, S. Siebentritt, *J. Phys. Condens. Matter* **2019**, 31, 425702.
[43] N. Barreau, P. Zabierowski, L. Arzel, M. Igalson, K. Macielak, A. Urbaniak, T. Lepetit, T. Painchaud, A. Dönmez, J. Kessler, *Thin Solid Films* **2015**, 582, 43.
[44] H. Elanzeery, M. Melchiorre, M. Sood, F. Babbe, F. Werner, G. Brammertz, S. Siebentritt, *Phys. Rev. Mater.* **2019**, 3, 055403.
[45] T. Kodalle, L. Choubrac, L. Arzel, R. Schlatmann, N. Barreau, C. A. Kaufmann, *Sol. Energy Mater. Sol. Cells* **2019**, 200, 109997.
[46] C. Stephan, S. Schorr, M. Tovar, H.-W. Schock, *Appl. Phys. Lett.* **2011**, 98, 091906.
[47] M. Malitckaya, H. P. Komsa, V. Havu, M. J. Puska, *J. Phys. Chem. C* **2017**, 121, 15516.
[48] T. Lepetit, S. Harel, L. Arzel, G. Ouvrard, N. Barreau, *Prog Photovolt.* **2017**, 25, 1068.
[49] M. Sood, H. Elanzeery, D. Adeleye, A. Lomuscio, F. Werner, F. Ehre, M. Melchiorre, S. Siebentritt, *Prog Photovolt.* **2020**, 28, 1063.
[50] S. Siebentritt, N. Rega, A. Zajogin, M. C. Lux-Steiner, *Phys. Status Solidi C* **2004**, 1, 2304.
[51] A. Bauknecht, S. Siebentritt, J. Albert, M. C. Lux-Steiner, *J. Appl. Phys.* **2001**, 89, 4391.
[52] C. Spindler, F. Babbe, M. H. Wolter, F. Ehré, K. Santhosh, P. Hilgert, F. Werner, S. Siebentritt, *Phys. Rev. Mater.* **2019**, 3, 090302.
[53] M. C. Artaud, F. Ouchen, L. Martin, S. Duchemin, *Thin Solid Films* **1998**, 324, 115.
[54] N. Rega, S. Siebentritt, I. E. Beckers, J. Beckmann, J. Albert, M. Lux-Steiner, *Thin Solid Films* **2003**, 431-432, 186.
[55] T. Irie, S. Endo, S. Kimura, *Jpn. J. Appl. Phys* **1979**, 18, 1303.
[56] R. Noufi, R. Axton, C. Herrington, S. K. Deb, *Appl. Phys. Lett.* **1984**, 45, 668.

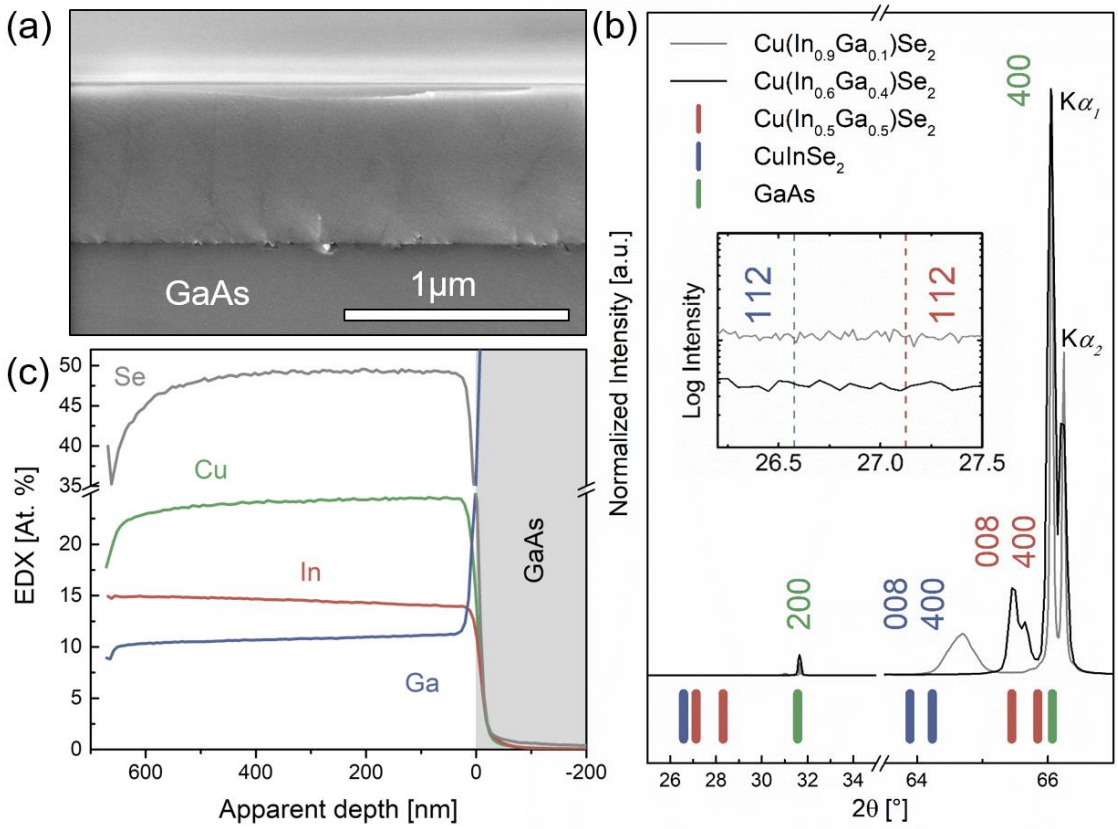

Figure 1. Cross-section SEM image of one of the samples used in this study showing no random grain boundaries (a). X-ray diffractogram of two samples showing the 008 reflection at different angles due to the difference in gallium content. Note the difference in scale after the break of 2θ axis. No reflection from the 112 planes can be observed in the logarithmic inset (b). Powder diffraction files number 00-014-045, 01-070-335 and 00-062-005 corresponding to GaAs, $CuInSe_2$ and $Cu(In_{0.5}Ga_{0.5})Se_2$, respectively, are used as references. Elemental profiles obtained by SIMS demonstrating that the single crystals have uniform distribution of the group III elements (c).

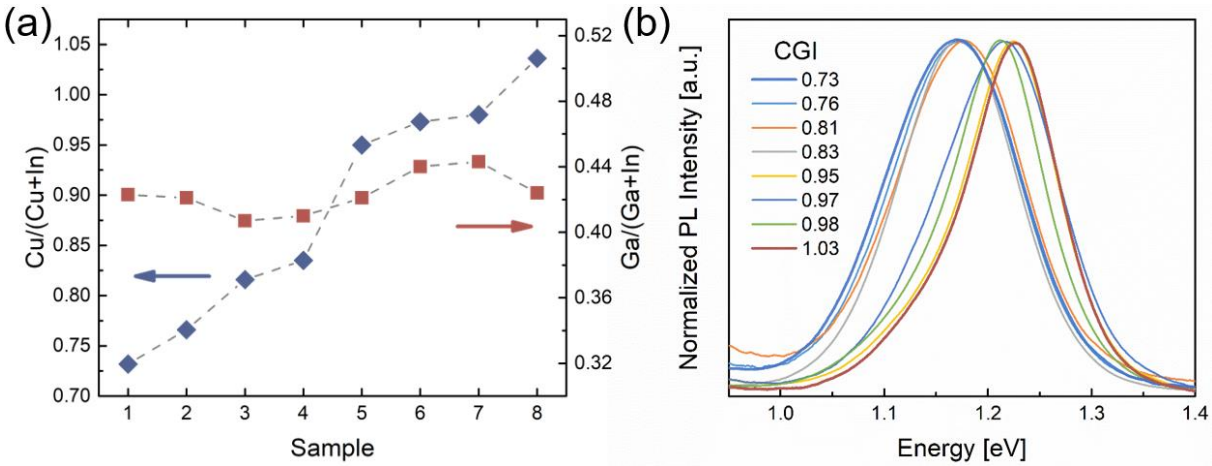

Figure 2. Cu/(Ga+In) and Ga/(Ga+In) ratios of all eight single crystals used for the investigation on the Cu content obtained from EDX, error bars show the standard deviation (a). Normalized room temperature PL of all samples (b). A difference of 60meV in bandgap due to the Cu and Ga content can be observed as well as a difference in the peak full width at half maximum when comparing the most Cu-poor and the close-to-stoichiometric sample.

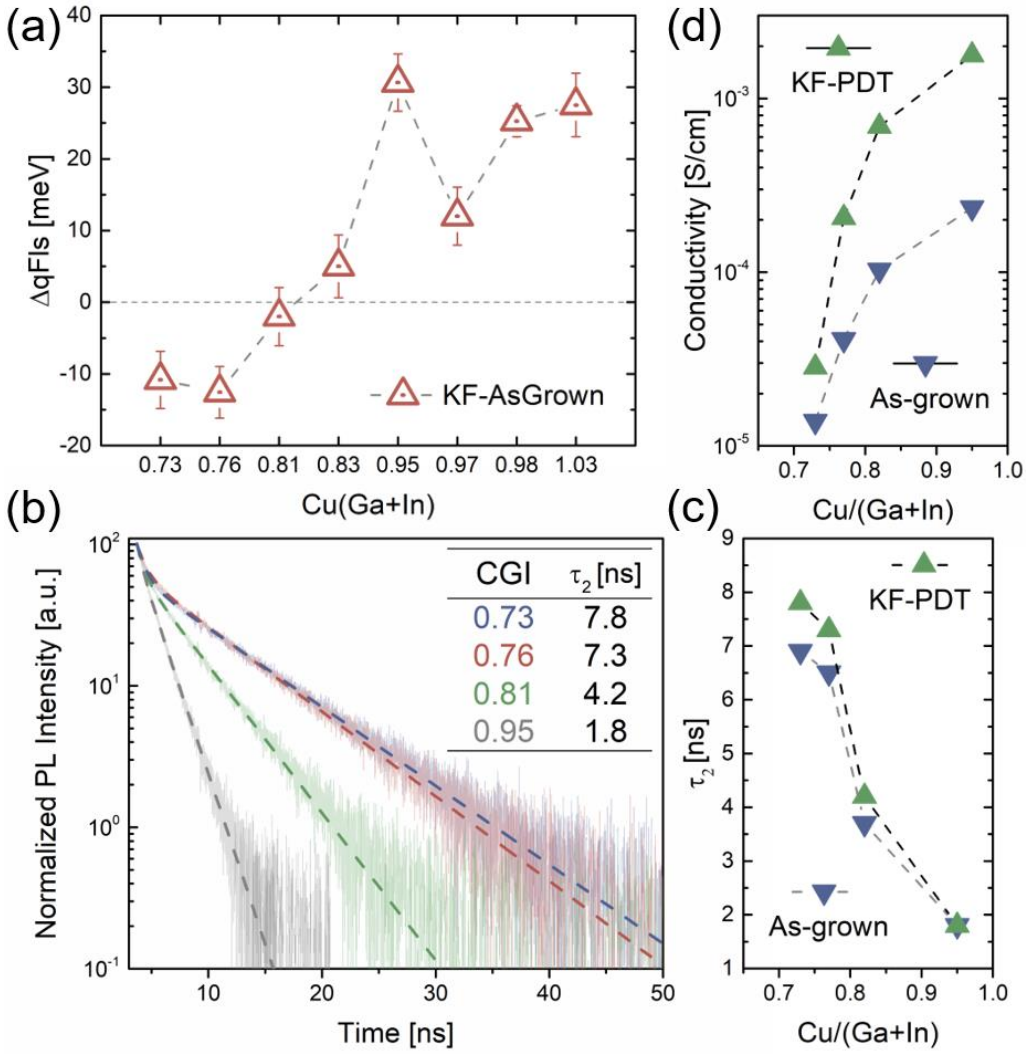

Figure 3. Quasi-Fermi level splitting difference (ΔqFls) obtained from subtracting the qFls of the as-grown from the qFls of the KF-treated samples, error bars account for the standard deviation of the data set, note the non-linear x axis (a). TRPL of four selected samples after receiving the KF-PDT (b). Comparison between the KF-treated and as-grown samples' lifetimes obtained from fitting the TRPL decays (c). Conductivity at room temperature of the same four samples comparing the KF-treated and as-grown state as well.

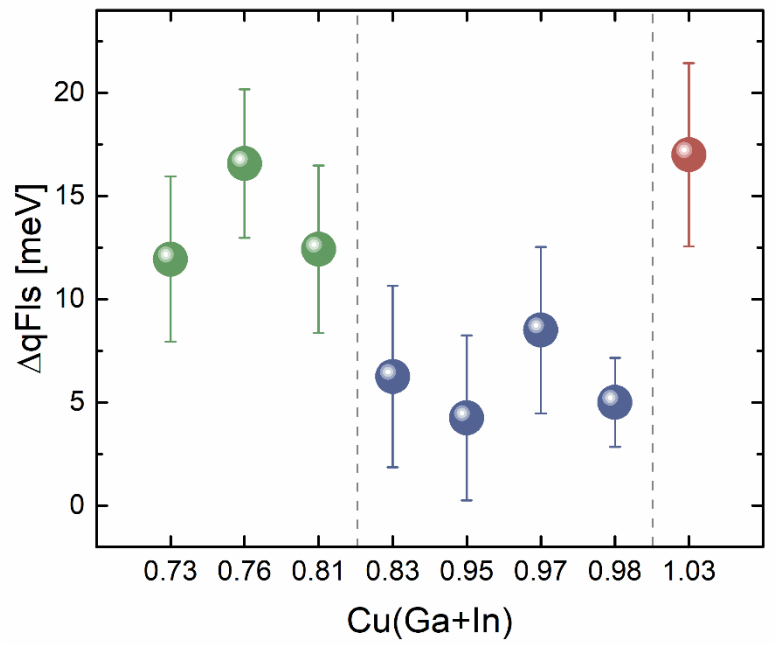

Figure 4. Quasi-Fermi level splitting difference (ΔqFls) between KF and Se-only treated absorbers with varying Cu content, note the non-linear x axis. Error bars indicate the standard deviation.

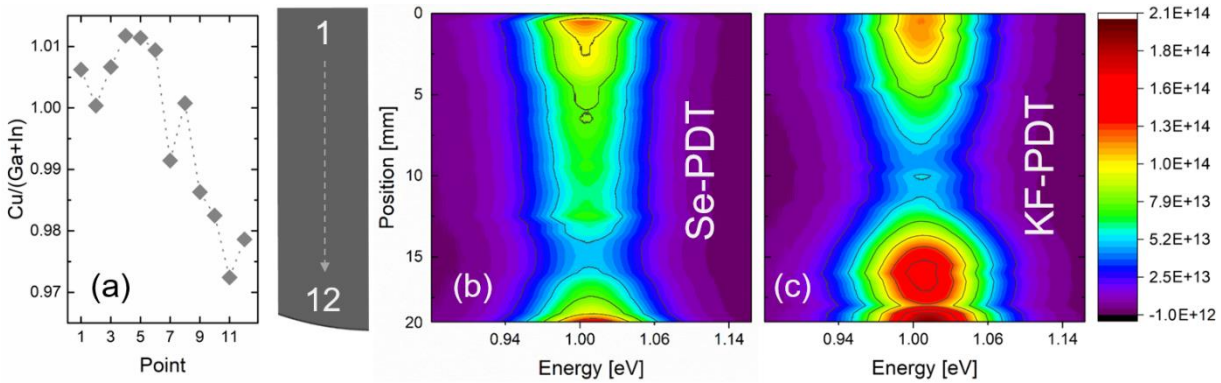

Figure 5. Cu/(Ga+In) measured along a close-to-stoichiometry sample with a radial compositional gradient and a schematic indicating the places of the measurements (a). PL maps of the same sample after receiving a Se-only (b) and KF-PDT(c). Larger improvement of the PL yield can be observer for the most Cu-poor side of the sample.

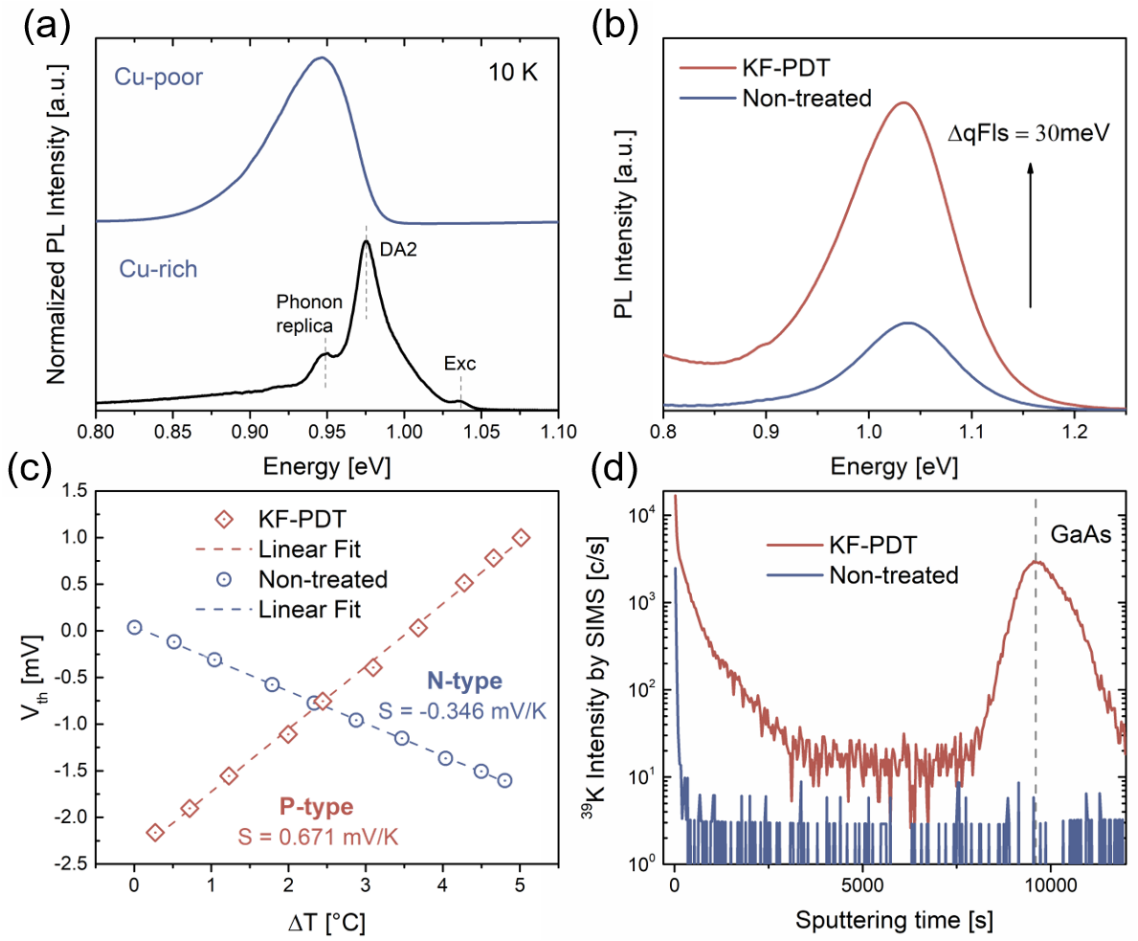

Figure 6. PL spectra of a Cu-poor and Cu-rich low gallium CIGSe at 10K (a). Room temperature PL of the Cu-poor sample after receiving the KF-PDT, the difference in PL intensity corresponds to an improvement of 30meV in qFls (b). Seebeck coefficient determination of the carrier type in the Cu-poor film before and after KF-PDT demonstrating a change in the type of conductivity (c). SIMS profile showing the potassium distribution along the film before and after KF-PDT (d).

Supporting Information

The effect of KF post-deposition treatments on the optoelectronic properties of Cu(In,Ga)Se_2 single crystals

Omar Ramírez, Maud Bertrand, Alice Debot, Daniel Siopa, Nathalie Valle, Jörg Schmauch, Michele Melchiorre and Susanne Siebentritt*

Table S1. Atomic percentages of all samples used in this study obtained from EDX and the calculated CGI and GGI ratios.

Sample No.	Name	Cu (At.%)	In (At.%)	Ga (At.%)	Se (At.%)	Cu/(In+Ga)	Ga/(Ga+In)
1	CIGSe265	20.7	16.3	11.9	51.2	0.73	0.42
2	CIGSe266	21.4	16.2	11.8	50.8	0.76	0.42
3	CIGSe269	22.4	16.3	11.2	50.3	0.81	0.41
4	CIGSe278	22.8	16.1	11.2	49.9	0.83	0.41
5	CIGSe268	24.6	15.0	10.9	49.6	0.95	0.42
6	CIGSe274	24.9	14.3	11.2	49.2	0.97	0.44
7	CIGSe282	24.9	14.1	11.3	49.8	0.98	0.44
8	CIGSe272	26.2	14.6	10.7	48.7	1.03	0.42
9	CIGSe251	23.2	24.8	2.0	50.0	0.86	0.08
10	CIGSe285	26.3	24.5	0.3	49.0	1.06	0.01
11	CIGSe280	27.6	23.9	0.7	47.8	1.12	0.03

Table S2. Quasi-Fermi level splitting measured at 10 suns of all samples used in the Cu-series for the three different conditions studied.

Sample No.	As-grown (meV)	Se-PDT (meV)	KF-PDT (meV)
1	686	663	675
2	693	664	681
3	674	660	672
4	698	697	703
5	669	695	700
6	666	669	678
7	691	711	716
8	665	676	693

Table S3. Quasi-Fermi level splitting difference (ΔqFls) between KF and Se-only PDT for CdS and Zn(O,S) buffer layers.

Sample No.	CdS (meV)	Zn(O,S) (meV)
6	9	9
8	17	12

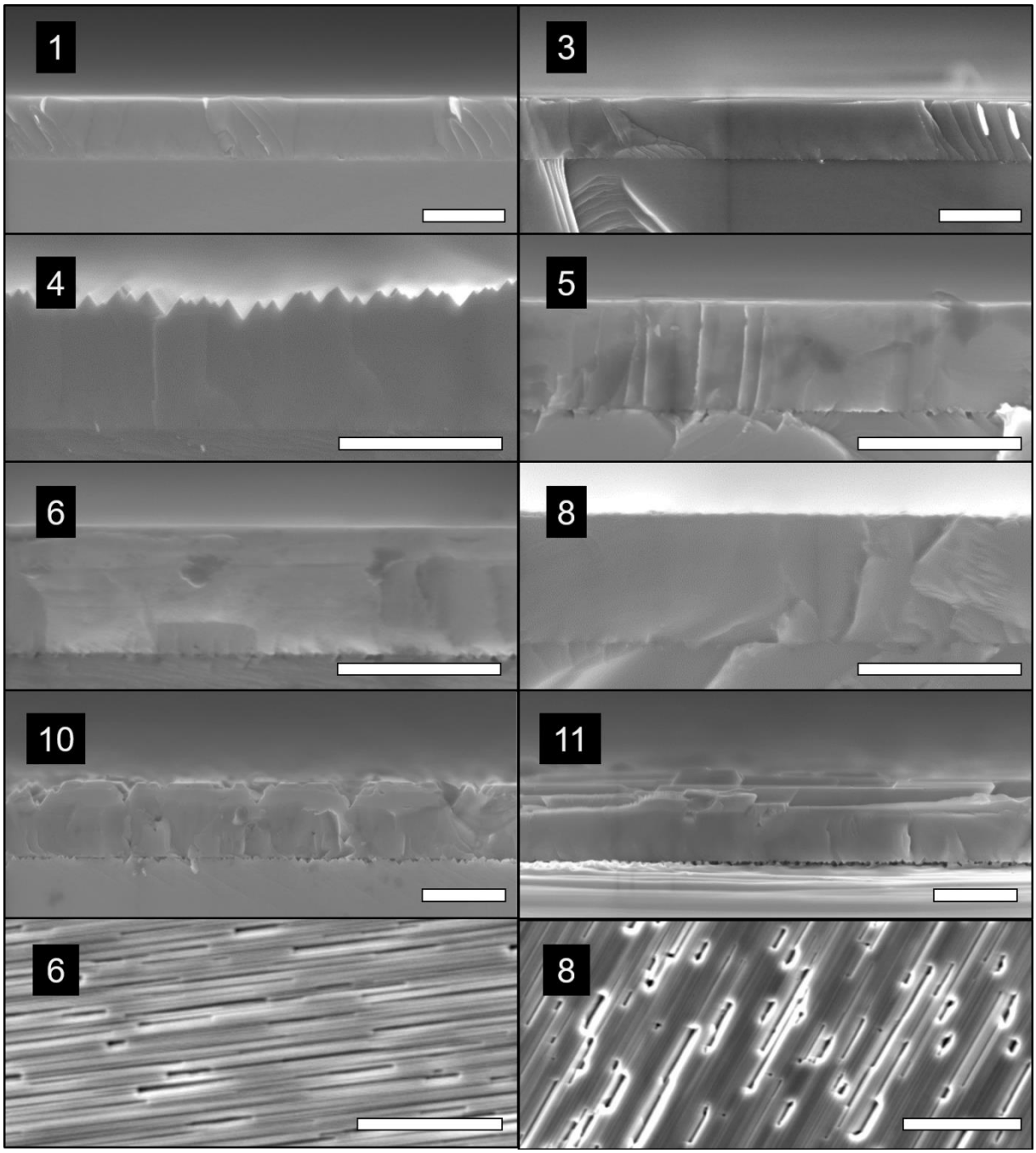

Figure S1. Cross-section and top-view SEM images, the numbers indicate the sample. For the cross-sections, the scale bar represents 1µm and for the top-views is 5µm. The strong faceting observed in part 4, 6, 8 and 10 is typical for Cu-poor or near-stoichiometric epitaxial films.

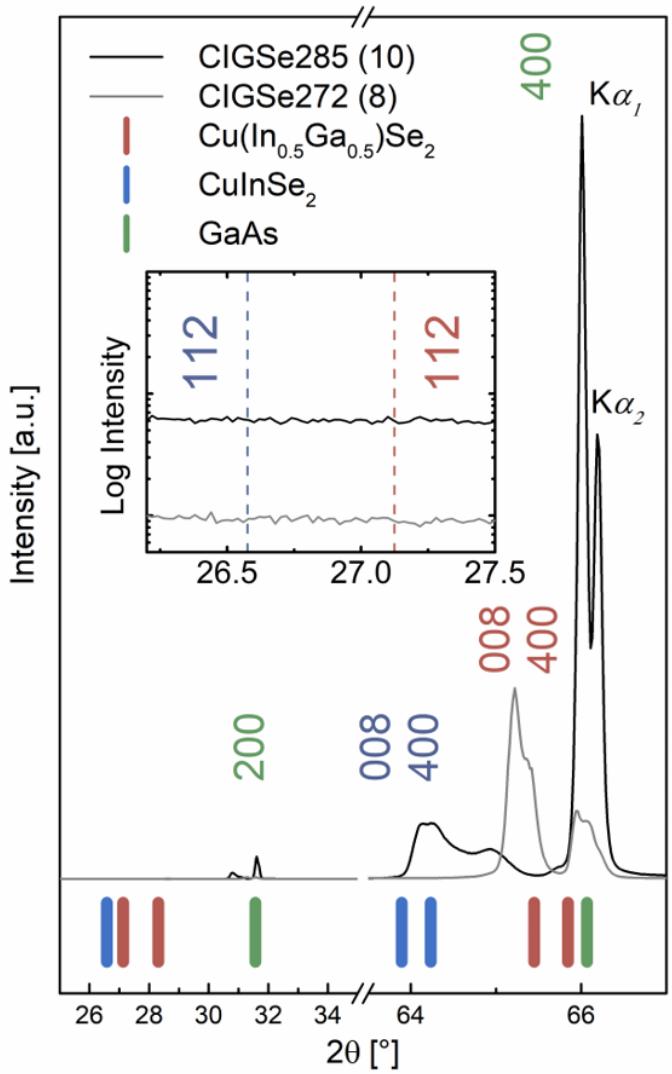

Figure S2.). X-ray diffractogram of samples 8 (GGI=0.42) and 10 (GGI=0.01) showing the 008 reflection at different angles due to the difference in gallium content. Note the difference in scale after the break of 2θ axis. No reflection from the 112 planes can be observed in the logarithmic inset. Powder diffraction files number 00-014-045, 01-070-335 and 00-062-005 corresponding to GaAs, $CuInSe_2$ and $Cu(In_{0.5}Ga_{0.5})Se_2$, respectively, are used as references.

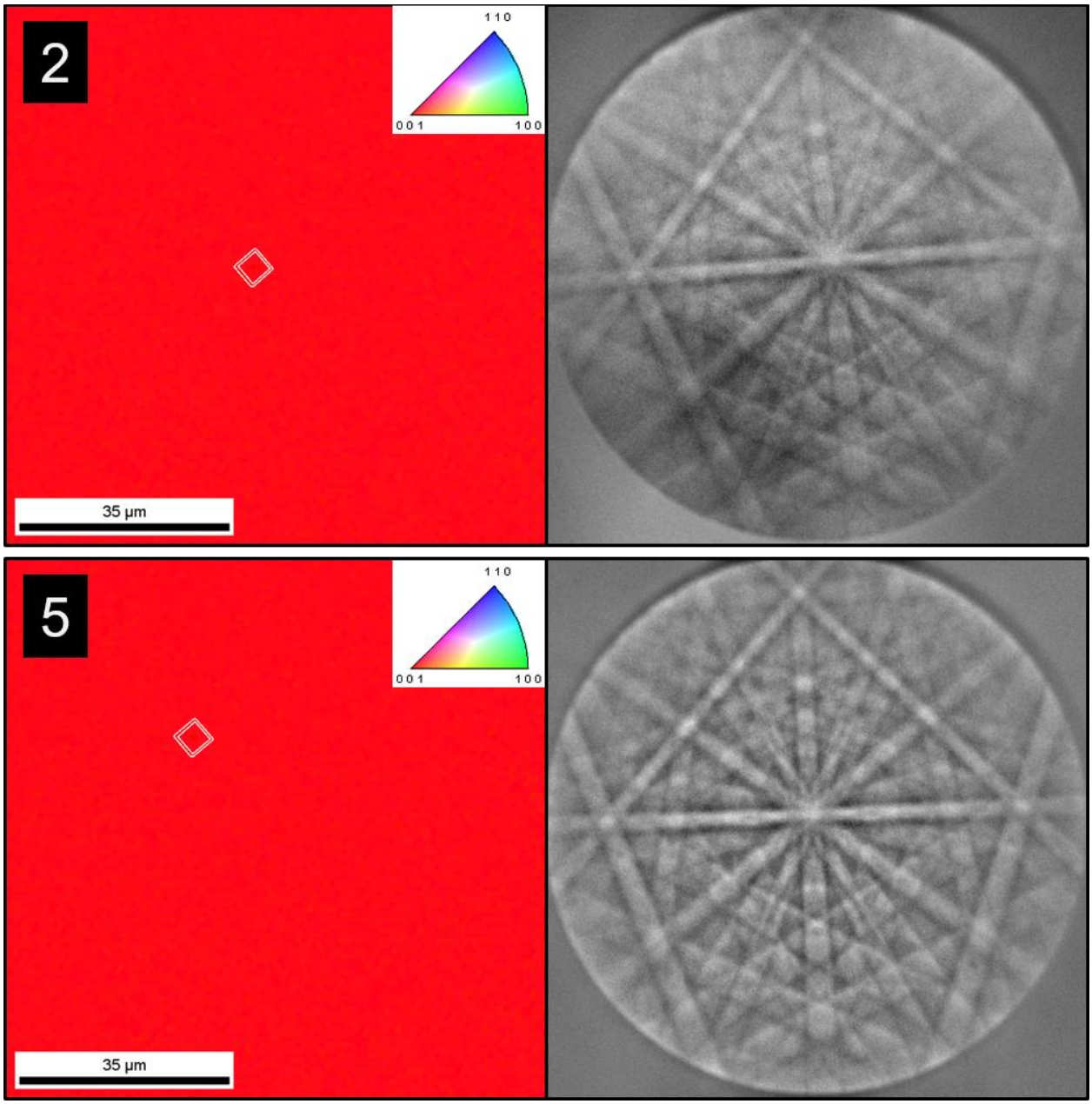

Figure S3. EBSD maps of two samples with different Cu content used in this study (sample number indicated in the black area) as well as the Kikuchi patterns obtained from the top-view. For the indexing of the EBSD maps, the JCPDS file number 351102 corresponding to a $CuIn_{0.7}Ga_{0.3}Se_2$ was used. From the inverse pole figures is possible to appreciate that no grain boundaries were detected over a large area.

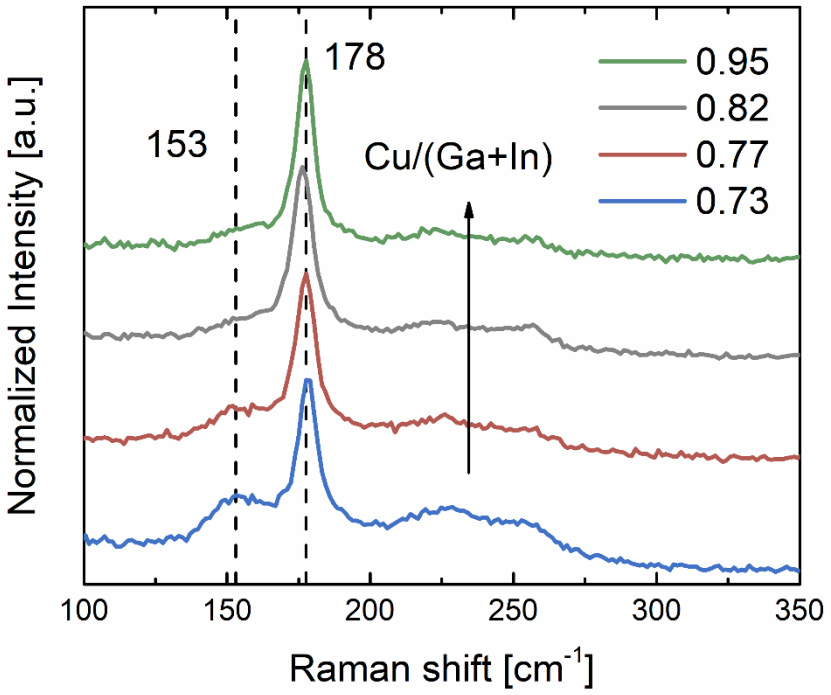

Figure S4. Raman spectra of four samples with different Cu content. The presence of an ordered vacancy compound was confirmed from the Raman shift at 153cm^{-1} in the samples with Cu content below 0.8. The peak at 178cm^{-1} corresponds to the chalcopyrite phase. The spectra are shifted vertically for clarity.

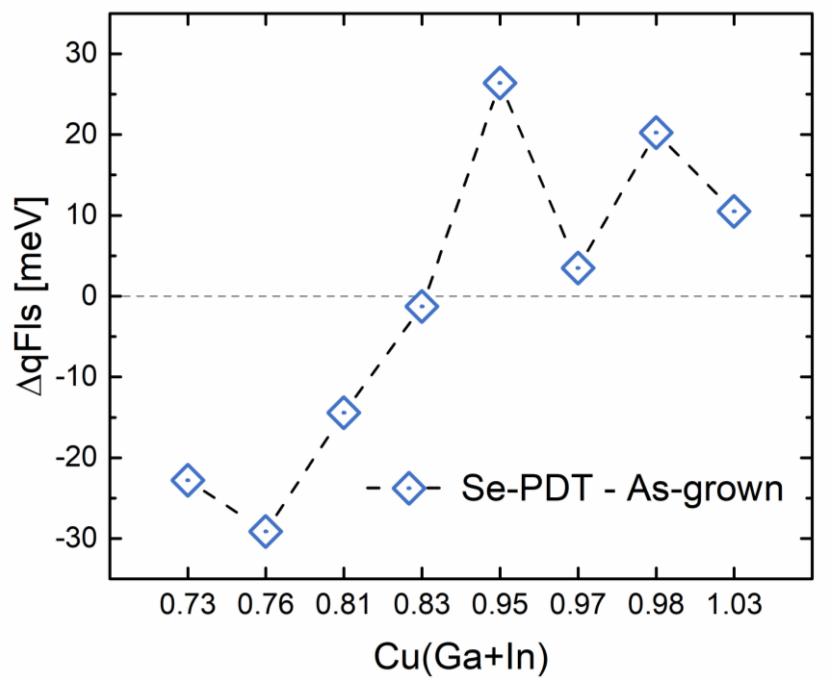

Figure S5. Quasi-Fermi level splitting difference (ΔqFls) between Se-treated and as-grown absorbers with varying Cu content, note the non-linear x axis.

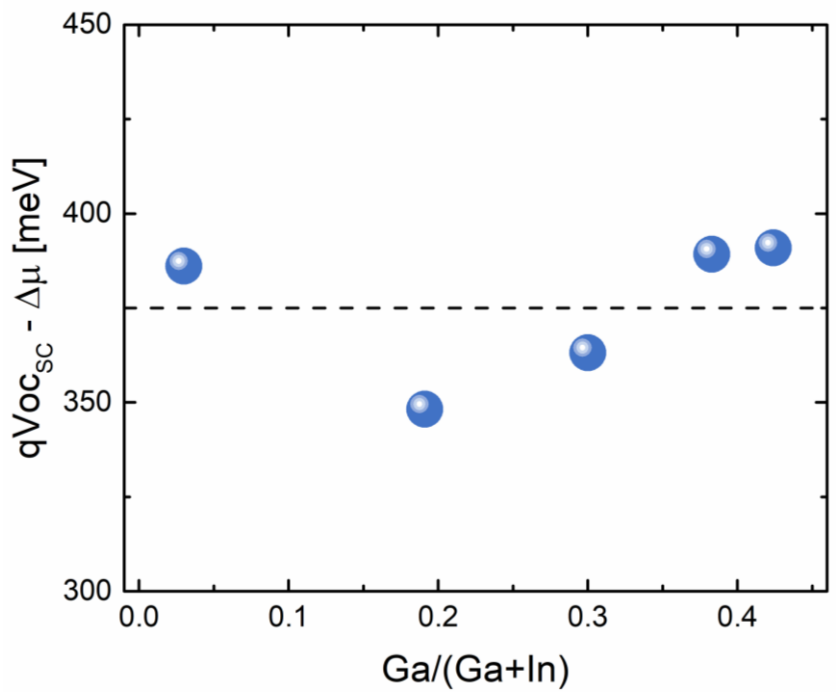

Figure S6. Quasi-Fermi level splitting loss with respect to the Shockley-Queisser V_{OC} for samples with different Ga content and similar Cu content under 10 son illumination. The bandgap used for the calculation was determined from the PL spectrum.

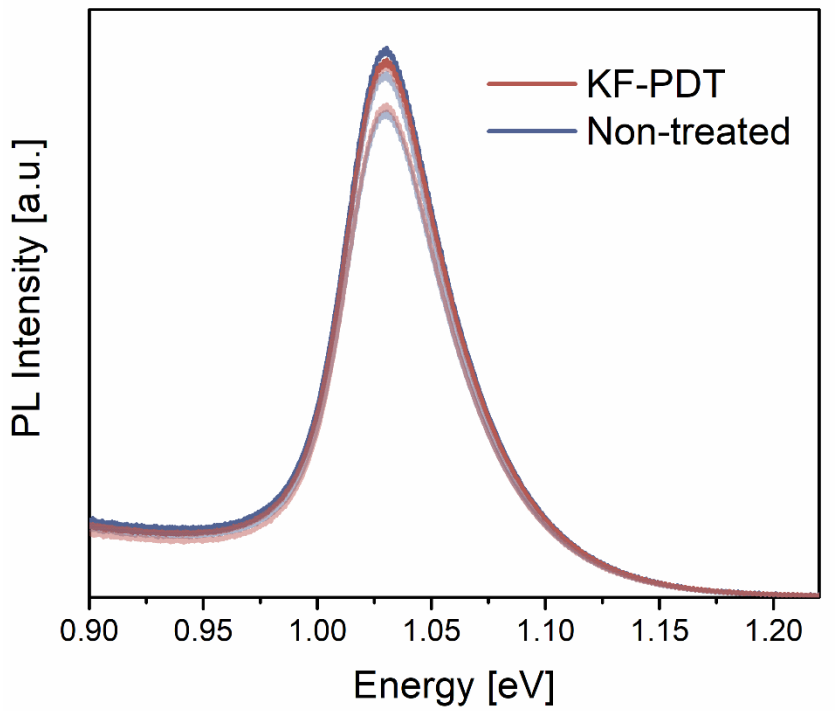

Figure S7. Room temperature PL spectra of Cu-rich low gallium CIGSe before and after KF-PDT.

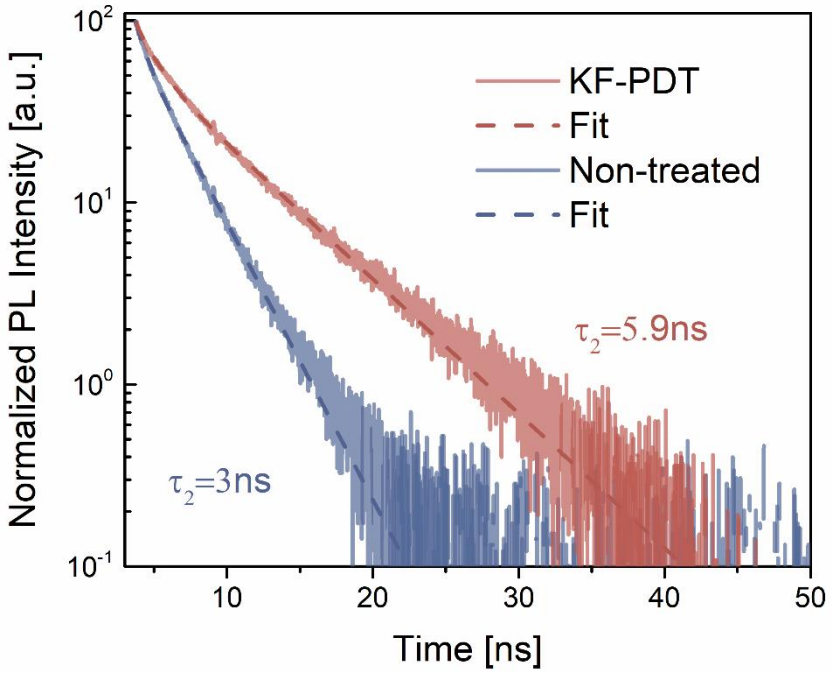

Figure S8. Measured TRPL decays and corresponding fits. The KF-PDT sample shows an improved minority carrier lifetime.